Design and Analysis of an Asymmetrically Fed Insulated Coaxial Slot Antenna with Enhanced Tip-Heating Performance

Lin-Kun Wu, *Member, IEEE,* and David Wen-Fong Su

***Abstract*—In this paper, a novel use of an asymmetrically fed insulated coaxial slot antenna (ICSA) type of applicator for interstitial microwave hyperthermia that simultaneously exhibits good impedance matching and enhanced tip-heating performances is presented. Theoretical analysis reveals that by making the distal arm much shorter than the other arm of the antenna, charge densities distributed over the distal arm of the antenna increase significantly. This, in turn, can result in the radial electric-field component becoming the dominant contributor to the specific absorption rate (SAR) over the distal arm side of the heating region and, therefore, the achievement of enhanced tip-heating performance. With the length of the longer arm chosen to be slightly longer than a quarter-wavelength, good impedance matching and enhanced tip-heating performances are achieved when the length of the shorter distal arm is reduced to no more than 25% of that of the longer arm. Good agreements observed between theoretical and measured SAR patterns for two ICSA's designed for operation at 915 and 433 MHz, respectively, confirm the validity of the design method.**

***Index Terms*—Asymmetrically fed insulated coaxial slot antenna, enhanced tip-heating performance, interstitial microwave hyperthermia, specific absorption rate.**

I. Introduction

INSULATED dipole antennas (IDA's) are widely used as applicators in the interstitial microwave hyperthermia treatments of deep-seated tumor and benign prostatic hyperplasia [1]–[3]. Two major factors determining the electrical performance of an insulated antenna are its input impedance and specific absorption rate (SAR) pattern characteristics. Good impedance matching is important and needed since tens of watts of microwave power is usually employed for raising tissue temperature to the hyperthermia level of 41 °C–50 °C.

In our earlier study [4], the input impedance model developed by King *et al.* [5] for IDA's was extended to the design of an insulated coaxial slot antenna (ICSA) type of applicator. Methods for optimizing the impedance-matching performance and for shortening the resonant length of an ICSA were described in detail in [4]. In this paper, a simple design method allowing an ICSA to achieve enhanced tip-heating performance is presented. The structural geometry of the ICSA concern here, which was designated as a CSA-II antenna in [4], is shown in Fig. 1. This antenna is constructed with the UT 78-50-25 triaxial cable from UTI (Micro-Coaxial Components, Collegeville, PA). Two sections of the antenna with lengths h_A and h_B, respectively, are fed by an annular slot. A quarter-wavelength choke provides an open-circuit termination to the backward current on Section B of the antenna.

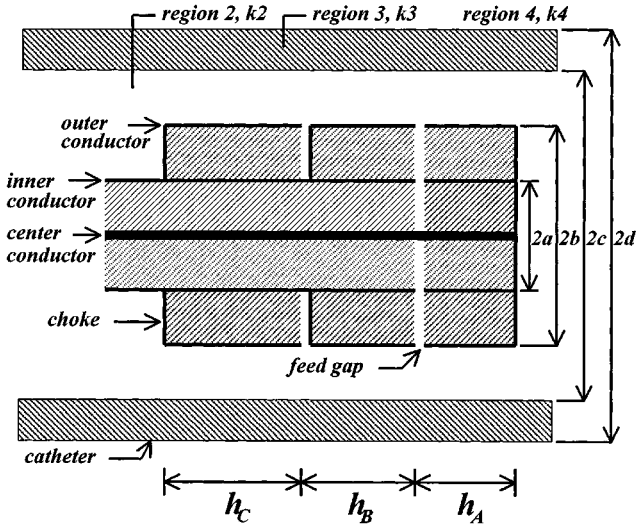

Fig. 1. Structural geometry of an ICSA.

As was demonstrated in [4] and [6], the installation of the choke circumvents the problems of insertion-depth-dependent antenna characteristics and undesired heating of the surface tissue near the point where an applicator is inserted [7], [8]. By making section length h_B clearly defined, both the impedance and radiation characteristics of the antenna become predictable through the methods described in [4] and [9]. In addition, the impedance model derived in [4] indicates that a multitude of arm lengths combinations (h_A, h_B) are generally available for the ICSA to achieve resonance at the intended ISM frequency of operation (e.g., 915 or 433 MHz). Since current distribution and radiated field distribution depend in part on (h_A, h_B) [5], [9], design of an ICSA that simultaneously achieves good impedance matching and a specific SAR pattern may be feasible by selecting a proper (h_A, h_B) combination.

Conventional IDA's, as were typified by, e.g., the designs of King *et al.* [5] and Camart *et al.* [10] are usually designed as

Manuscript received May 14, 1999. This work was supported by the National Research Council of the Republic of China under Grant NSC 87-2213-E-009-127.

L.-K. Wu is with the Institute of Communication Engineering, National Chiao Tung University, Hsinchu, Taiwan 30050, R.O.C.

D. W-F. Su was with the Institute of Communication Engineering, National Chiao Tung University, Hsinchu, Taiwan 30050, R.O.C. He is now with Alpha Telecom Inc., Hsinchu, Taiwan 30050, R.O.C.

Publisher Item Identifier S 0018-9480(00)06546-7.

broadside applicators. The radiated energy is predominantly deposited around the feed gap. Hence, in order to achieve an effective heating of the malignant tissue, an applicator is usually inserted in a way that its distal end may extrude beyond a tumor, which, therefore, subjects the surrounding healthy tissue to the threats of unnecessary heating and mechanical destruction. To circumvent this problem, an applicator with an enhanced tip-heating characteristic is required.

Turner [11] and Tumeh and Iskander [12] had investigated the uses of multisectioned dipoles for adjusting the longitudinal SAR distribution. In these cases, the dipole is divided into a number of sections of different diameters. From the King *et al.* theory of IDA [5], sections with larger diameters will have more power being absorbed by the surrounding lossy tissues. This effect is accounted for by an empirically derived section-dependent radiation efficiency term in [12] when summing the contributions to the radiated field from different sections. Although results obtained in [11] and [12] indicate that adjustment of a longitudinal SAR pattern can be achieved with a properly designed multisectioned IDA, its design procedure is not all that straightforward and its mechanical construction appears to be complicated.

In another design example, a shielding technique was applied by Camart *et al.* [13] to confine the longitudinal heating extent of a dipole insulated by a double-layered catheter. This research was motivated by the need to obtain a SAR pattern with a longitudinal extent comparable to that of the region to be heated (e.g., around 2 cm for the BPH treatment considered in [13]) from an applicator of much longer length. In this case, a "ringed" applicator is obtained by the coating of metallic rings on the external wall of the inner layer of the catheter. By effectively suppressing radiation from the shielded portions of the insulated antenna, the effective radiation length and resulting longitudinal extent are much shorter than the physical length of the applicator. To be successful, effects of metallic rings on both the input impedance and SAR pattern have to be modeled during the applicator's design stage.

In [14] and [15], Lin and Wang developed a balun-fed folded dipole antenna to achieve enhanced heating beyond the tip of the applicator at 2.45 GHz. In this design, the two arms of the dipole are, respectively, connected to the inner and outer conductors of the input coaxial cable. A quarter-wavelength choke is attached to the outer conductor of the coaxial cable to form the balun. For practical purposes, however, the two arms of the dipole, both of length 3 mm, are folded back toward the input coaxial cable (it is thus named a folded dipole) such that their ends are spaced 1 mm away from the opening of the choke. Temperature measurements made in the saline-filled test tube indicate that peak power deposition occurs within a longitudinal extent of about 0 to 3 mm "beyond" the tip; as such, Cerri *et al.* [16] referred it as a thermic "end-fire" applicator. While heating at a radial distance of 1 mm from the tip is 50% higher than the rest of the antenna, at 2 mm, tip heating is the same as elsewhere. The highly localized heating pattern is a result of both antenna design and high operating frequency used. Although this antenna is appropriate for such a precision interstitial treatment as cardiac ablation, it is inconvenient for treating larger tumors for which a large antenna array is required.

In [16], Cerri *et al.* investigated the use of a coaxial slot antenna to achieve the thermic end-fire characteristics at 2.45 GHz. It is noted that this antenna is immediately surrounded by an ambient lossy medium without any insulating catheter or dielectric coating. For the specific design example presented in [16], although peak power deposition did occur slightly beyond the tip, a heating pattern was also found to extent back along the input coaxial cable. This may be attributed in part to the lack of choke, which results in the radiation from the inevitable backward current flowing on the exterior surface of the outer conductor of the input coaxial cable, and in part to the heat propagates backward along the cable faster than in the phantom. The latter is a combined result of the -6-dB return loss obtained at the operating frequency and the high value of the thermal conductivity of the copper.

In this paper, a novel use of an asymmetrically fed ICSA for achieving enhanced tip-heating performance is presented. Theoretical prediction of SAR patterns, conditions required for achieving enhanced tip-heating performance and the underlying physics, are described in detail in Section II. This is followed by experimental verifications in Section III and concluding remarks in Section IV.

II. Theoretical Analysis

According to [9] and [12], the electromagnetic fields radiated by an insulated dipole embedded in a homogeneous lossy medium can be predicted directly from the distribution of current on the conductor. It was further demonstrated in [9] that for an IDA, the longitudinal SAR distribution generally resembles that of the current distribution. However, while exercising the resonant-length-shortening concept advanced in [4] for the design of ICSA's, it was discovered that longitudinal SAR distribution no longer follows that of the current distribution and, more interestingly, enhanced tip-heating performance may start appearing when the ICSA becomes extremely asymmetrically fed. This behavioral change is demonstrated in Fig. 2 by the theoretical SAR distributions computed at 915 MHz using the method presented in [9] for four ICSA's with a common h_B of 40 mm and different h_A's of 40, 30, 20, and 10 mm. The corresponding normalized current distributions are shown in Fig. 3. By examining the corresponding cases shown in Figs. 2 and 3, it becomes obvious that additional insights into the longitudinal shift of peak SAR observed for the ICSA with $h_A = 10$ mm must be sought.

The electric field radiated by an insulated dipole has a longitudinal component E_z and a radial component E_ρ. Together they determine the SAR

$$\mathrm{SAR} = \frac{\sigma}{\rho_m}\left(|E_z|^2 + |E_\rho|^2\right) \tag{1}$$

where σ and ρ_m are, respectively, the electrical conductivity and mass density of the surrounding lossy medium.

Near-field physics indicates that since E_z points in a direction parallel to the axis of the dipole, it is related to the axial current distribution $\vec{J} = \hat{z}J_z(z')$, $-h_B \le z' \le h_A$. On the other hand, E_ρ, which is normal to the axis of dipole, is related to the charge distribution $\rho(z')$. In the design of an insulated antenna, $J_z(z')$

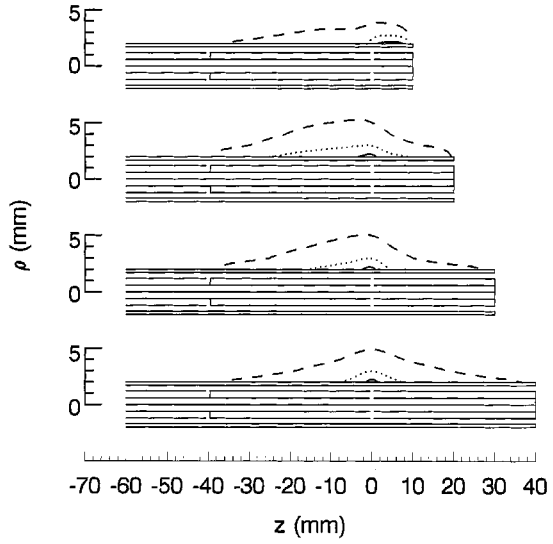

Fig. 2. Theoretical SAR distributions computed at 915 MHz for four ICSA's with a common h_B of 40 mm and different h_A's of 40, 30, 20, and 10 mm. Solid line: 90% SAR. Dotted line: 60% SAR. Dashed line: 30% SAR.

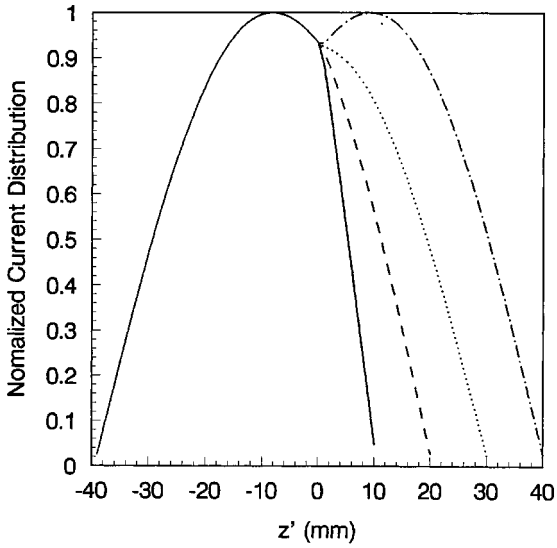

Fig. 3. Normalized current distributions associated with the four ICSA's considered in Fig. 2. Solid line: $h_A = 10$ mm. Dashed line: $h_A = 20$ mm. Dotted line: $h_A = 30$ mm. Dotted–dashed line: $h_A = 40$ mm.

is determined first by following King *et al.*'s IDA theory [4], [5]. Now, by invoking the equation of continuity, $\rho(z')$ can be found from

$$\rho(z') = \frac{j}{\omega}\frac{dJ_z(z')}{dz'}. \tag{2}$$

Considering the symmetrically fed IDA analyzed by King *et al.* [5] as an example, radiated electric-field components can be expressed as

$$E_z = \frac{j\omega\mu_0 I(0)}{4\pi \sin k_L h} \cdot \left\{ \left(1 - \frac{k_L^2}{k_4^2}\right) \cdot \int_0^h \sin k_L(h - z') \cdot \Big[\Phi(z, z') + \Phi(z, -z')\Big] dz' + \frac{k_L}{k_4^2} \cdot \Big[\Phi(z, h) + \Phi(z, -h) - 2\Phi(z, 0)\cos k_L h\Big] + \frac{1}{2}\left(\frac{k_L^2}{k_{2e}^2 - 1}\right) d^2 \ln\frac{d}{a} \int_0^h \sin k_L(h - z') \frac{\partial^2}{\partial \rho^2} \cdot \Big[\Phi(z, z') + \Phi(z, -z')\Big] dz' \right\} \tag{3}$$

$$E_\rho = \frac{j\omega\mu_0 I(0)}{4\pi \sin k_L h} \left\{ \left(\frac{k_L \rho}{k_4^2}\right) \cdot \int_0^h \cos k_L(h - z') \cdot \left[\left(\frac{-jk_4}{R_1} - \frac{1}{R_1^2}\right)\Phi(z, z') + \left(\frac{-jk_4}{R_2} + \frac{1}{R_2^2}\right)\Phi(z, -z') \right] dz' - \frac{1}{2}\left(\frac{k_L^2}{k_{2e}^2} - 1\right) k_L\, d^2 \ln\frac{d}{a} \cdot \int_0^h \cos k_L(h - z') \frac{\partial}{\partial \rho} \cdot [\Phi(z, z') - \Phi(z, -z')] dz' \right\} \tag{4}$$

where the complex propagation constant k_4 and effective wavenumber k_{2e} can be found in [5], $\Phi(z, z')$ is defined as

$$\Phi(z, z') = \frac{e^{-jk_4 R_1}}{R_1} \tag{5}$$

and

$$R_1 = \Big[(z - z')^2 + \rho^2\Big]^{1/2} \tag{6}$$

$$R_2 = \Big[(z + z')^2 + \rho^2\Big]^{1/2}. \tag{7}$$

Since $J_z(z')$ assumes a sinusoidal distribution, it then follows that $\rho(z')$ has a cosinusoidal form. Therefore, the $\sin k_L(h - z')$ and $\cos k_L(h - z')$ terms appearing in (3) and (4), respectively, indicate that E_z is indeed governed by $J_z(z')$ while E_ρ is governed by $\rho(z')$. As a consequence, depending on the construction of the antenna, either $|E_z|$ or $|E_\rho|$ can be the dominant contributor to SAR, and since the shapes of current and charge distributions are not the same, the resulting longitudinal SAR distributions are different.

To see how charge distribution may affect the SAR pattern, normalized charge distributions are computed and plotted in Fig. 4 for the four ICSA's considered in Figs. 2 and 3. For the symmetrically fed ICSA, maximum charge distributions $|\rho(z')|$ are found at the distal end of both Sections A and B. For the asymmetrically fed ICSA with $h_A = 30$ mm, maximum $|\rho(z')|$ occurs at the distal end of Section B. However, for shorter h_A's of 20 and 10 mm, maximum $|\rho(z')|$ occurs at the distal end of Section A. Of particular interest is that, for the extreme case of $h_A = 10$ mm, charge distribution becomes much larger over Section A than over Section B of the antenna. This, as was explained earlier, should lead to much stronger $|E_\rho|$'s to be present over the Section A side of the heating region.

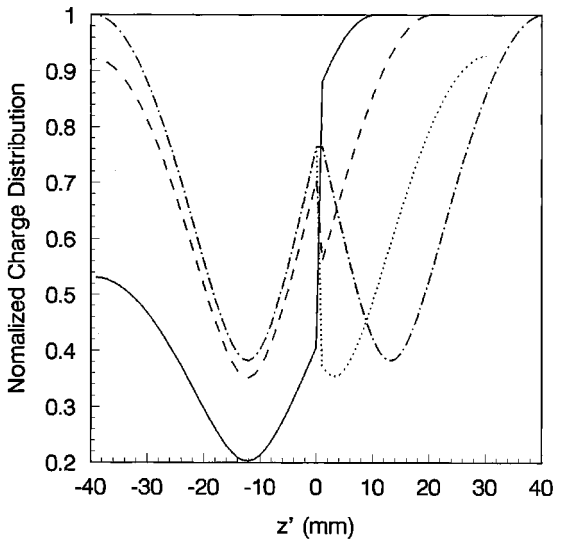

Fig. 4. Normalized charge distributions associated with the four ICSA's considered in Fig. 2. Solid line: $h_A = 10$ mm. Dashed line: $h_A = 20$ mm. Dotted line: $h_A = 30$ mm. Dotted–dashed line: $h_A = 40$ mm.

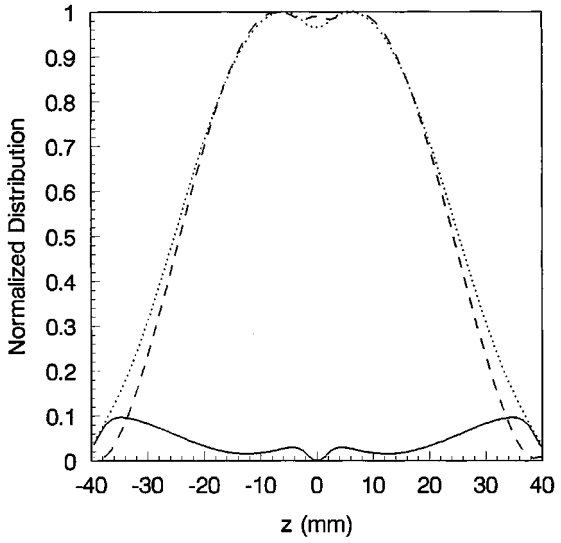

Fig. 5. Longitudinal variations of the normalized $|E_\rho|^2$, $|E_z|^2$, and SAR computed at $\rho = 2$ mm for the symmetrically fed ICSA with $h_A = h_B = 40$ mm. Solid line: $|E_\rho|^2$. Dashed line: $|E_z|^2$. Dotted line: SAR.

To explore this further, longitudinal variations of the normalized $|E_z|^2$, $|E_\rho|^2$, and SAR computed at $\rho = 2$ mm for the symmetrically fed ICSA's are shown in Fig. 5. As can be seen, the SAR distribution with peaks at $z = \pm 6.5$ mm is dominated by $|E_z|^2$, which has a shape closely resembling that of the corresponding current distribution shown in Fig. 2. For comparison, corresponding data obtained for the extremely asymmetrically fed ICSA with $h_A = 10$ mm are plotted in Fig. 6. In this case, SAR distribution is dominated by $|E_\rho|^2$ when $z > 0$, while by $|E_z|^2$ when $z < 0$. More importantly, since maximum $|E_\rho|^2$ is about twice as large as the maximum $|E_z|^2$, SAR's are found to be much larger over the $z > 0$ region than the $z < 0$ region. This enhanced tip-heating characteristic is clearly due to the significantly reduced h_A, which results in significant increases in the corresponding $\rho(z')$ and $|E_\rho|$.

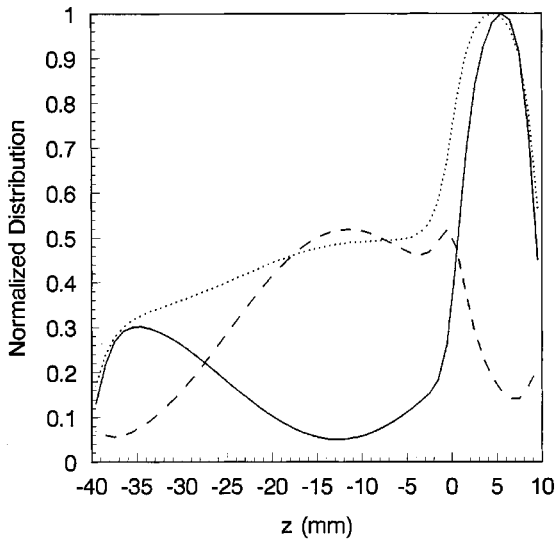

Fig. 6. Longitudinal variations of the normalized $|E_\rho|^2$, $|E_z|^2$, and SAR computed at $\rho = 2$ mm for the extremely asymmetrically fed ICSA with $h_A = 10$ mm and $h_B = 40$ mm. Solid line: $|E_\rho|^2$. Dashed line: $|E_z|^2$. Dotted line: SAR.

III. Experimental Results

In order to verify the enhanced tip-heating capability predicted in Section II, two ICSA's are designed by applying the technique of using extra internal current path to shorten the resonant length of an ICSA [4] and the asymmetrical-feeding principle described in Section II to resonate at 915 and 433 MHz, respectively, for experimental verifications. Both antennas are constructed with the UT 78-50-25 triaxial cable from UTI (Micro-Coax Components). A PTFE catheter with 2.0-mm inner diameter and 3.2-mm outer diameter is used to house these antennas. They are then inserted through a pre-drilled hole into a solid muscle-equivalent phantom, which is composed of 58.33% ethanediol, 36.67% H_2O, 1.67% NaCl, and 3.33% agar (weight percents) [4]. The complex permittivities of the mixture measured at 433 and 915 MHz using the HP85010 dielectric constant measurement system are $48.74 - j30.74$ and $47.29 - j22.26$, respectively. The measured SAR patterns shown in Figs. 7 and 8 are calculated from the temperature maps recorded by an infrared camera on the bisected phantom before and after the application of 10 W of microwave power for 20 s.

For the 915-MHz case, the designed ICSA with $h_A = 10$ mm and $h_B = 40$ mm exhibits a theoretical $|S_{11}|$ of -25 dB and the measured $|S_{11}|$ of -23 dB. The h_A/h_B ratio is 0.25. The measured SAR pattern shown in Fig. 7 clearly confirms the theoretically predicted enhanced tip-heating performance. When compared to the calculated data shown in Fig. 2, good agreement between calculated and measured results are observed. By following the same design procedure, a 433-MHz ICSA with $h_A = 16$ mm and $h_B = 80$ mm (i.e., $h_A/h_B = 0.2$) is obtained. The calculated and measured $|S_{11}|$ are -18 and -21 dB, respectively. For the measured SAR pattern shown in Fig. 8, the longitudinal extent of the 30% SAR distribution is found to coincide with the 10-mm length of Section B of the antenna.

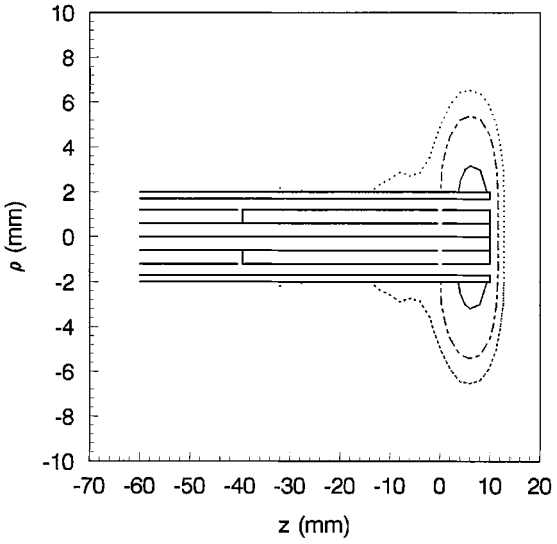

Fig. 7. Measured SAR pattern for the 915-MHz ICSA with $h_A = 10$ mm and $h_B = 40$ mm. Solid line: 90% SAR. Dotted–dashed line: 50% SAR. Dotted line: 30% SAR.

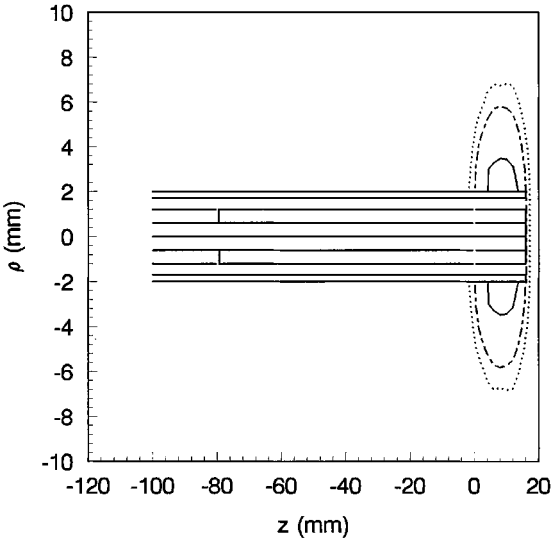

Fig. 8. Measured SAR pattern for the 433-MHz ICSA with $h_A = 16$ mm and $h_B = 80$ mm. Solid line: 90% SAR. Dotted–dashed line: 50% SAR. Dotted line: 30% SAR.

In summary, proper uses of a resonant-length shortening technique and asymmetrical-feeding arrangement have resulted in the two ICSA's to exhibit simultaneous good impedance matching and enhanced tip-heating performances. Although the lower frequency of operation demands a larger physical length for the 433-MHz ICSA, the smaller h_A/h_Bratio used results in an even more confined longitudinal SAR extent for the 433-MHz ICSA.

IV. Conclusions

The fact that there exists a multitude of (h_A, h_B) combinations for ICSA to achieve resonance at the desired frequency of operation has been exploited in this paper in the design of an asymmetrically fed ICSA that simultaneously achieves good impedance matching and enhanced tip-heating performances. While localized heatings beyond the tip were achieved in [14]–[16], it occurs over the tip (or distal) section of the ICSA investigated here. In view of this, the ICSA examined here functions as "thermic broadside" applicator and it should be inserted in a way that its tip is in direct contact with the outer boundary of the region to be heated. In addition, by designing for operation at lower ISM frequencies, our ICSA's also produce larger radial heating extent than the 2.45-GHz applicators considered in [14]–[16]. Thus, it suggests that fewer elements are needed when constructing an applicator array to heat large-sized tumor.

Theoretical analysis has revealed that for a given h_B, reducing h_A results in an increase in the charge density over Section A of the antenna, which, in turn, causes the corresponding $|E_\rho|$ to increase. Once a sufficient shortening of h_A has been achieved, $|E_\rho|$ becomes the dominant contributor to SAR and enhanced tip-heating results. For the structural and material parameters used here with h_B chosen to be slightly longer than a quarter-wavelength, a simple criterion of $h_A/h_B < 0.25$ has been found both theoretically and experimentally to produce excellent tip-heating performance. When different antenna types (e.g., IDA) and materials (e.g., cable, catheter, and tissue) are involved in the design of insulated antenna to achieve good impedance matching and enhanced tip-heating performances, which are insertion-depth independent, methods presented in this paper and in [4] and [9] may be advantageously consulted.

References

[1] B. E. Lyons, R. H. Britt, and J. W. Strohbehn, "Localized hyperthermia in the treatment of malignant brain tumors using an interstitial microwave antenna array," *IEEE Trans. Biomed. Eng.*, vol. BME-31, pp. 53–62, Jan 1984.

[2] A. M. Tumeh and M. F. Iskander, "Performance comparison of available interstitial antennas for microwave hyperthermia," *IEEE Trans. Microwave Theory Tech.*, vol. 37, pp. 1126–1133, July 1989.

[3] D. Despretz, J.-C. Camart, C. Michel, J.-J. Fabre, B. Prevost, J.-P. Sozanski, and M. Chive, "Microwave prostatic hyperthermia: Interest of urethral and rectal applicators combination—Theoretical study and animal experimental results," *IEEE Trans. Microwave Theory Tech.*, vol. 44, pp. 1762–1767, Oct. 1996.

[4] D. W.-F. Su and L. K. Wu, "Input impedance characteristics of coaxial slot antennas for interstitial microwave hyperthermia," *IEEE Trans. Microwave Theory Tech.*, vol. 47, pp. 302–307, Mar. 1999.

[5] R. W. P. King, B. S. Trembly, and J. W. Strohbehn, "The electromagnetic field of an insulated antenna in a conducting or dielectric medium," *IEEE Trans. Microwave Theory Tech.*, vol. MTT-31, pp. 574–583, July 1983.

[6] W. Hurter, F. Reinbold, and W. J. Lorenz, "A dipole antenna for interstitial microwave hyperthermia," *IEEE Trans. Microwave Theory Tech.*, vol. 39, pp. 1048–1054, Jun. 1991.

[7] Y. Zhang, N. V. Dubal, R. Takemoto-Hambleton, and W. T. Joines, "The determination of the electromagnetic field and SAR pattern of an interstitial applicator in a dissipative dielectric medium," *IEEE Trans. Microwave Theory Tech.*, vol. 36, pp. 1438–1443, Oct. 1988.

[8] G. B. Gentili, M. Leoncini, B. S. Trembly, and S. E. Schweizer, "FDTD electromagnetic and thermal analysis of interstitial hyperthermic applicators," *IEEE Trans. Biomed. Eng.*, vol. 42, pp. 973–980, Oct. 1995.

[9] L. K. Wu, D. W.-F. Su, and B.-C. Tseng, "A fast algorithm for computing field radiated by an insulated dipole antenna in dissipative medium," *IEEE Trans. Microwave Theory Tech.*, vol. 44, pp. 2290–2293, Dec. 1996.

[10] J.-C Camart, J.-J. Fabre, B. Prevost, J. Pribetich, and M. Chive, "Coaxial antenna array for 915 MHz interstitial hyperthermia: Design and modelization—power deposition and heating pattern—phased array," *IEEE Trans. Microwave Theory Tech.*, vol. 40, pp. 2243–2250, Dec. 1992.

[11] F. Turner, "Interstitial equal-phased arrays for EM hyperthermia," *IEEE Trans. Microwave Theory Tech.*, vol. MTT-34, pp. 572–578, May 1986.

[12] A. M. Tumeh and M. F. Iskander, "Performance comparison of available interstitial antennas for microwave hyperthermia," *IEEE Trans. Microwave Theory Tech.*, vol. 37, pp. 1126–1133, July 1989.
[13] J.-C. Camart, D. Despretz, M. Chive, and J. Pribetich, "Modeling of various kinds of applicators used for microwave hyperthermia based on the FDTD method," *IEEE Trans. Microwave Theory Tech.*, vol. 44, pp. 1811–1818, Oct. 1996.
[14] J. C. Lin and Y. Wang, "Interstitial microwave antennas for thermal therapy," *Int. J. Hyperthermia*, vol. 3, no. 1, pp. 37–47, 1987.
[15] ——, "An implantable microwave antenna for interstitial hyperthermia," *Proc. IEEE*, vol. 75, pp. 1132–1133, Aug. 1987.
[16] G. Cerri, R. De Leo, and V. M. Primiani, "'Thermic end-fire' interstitial applicator for microwave hyperthermia," *IEEE Trans. Microwave Theory Tech.*, vol. 41, pp. 1135–1142, June 1993.

Lin-Kun Wu (S'81–M'81) was born in Hsinchu, Taiwan, R.O.C., in 1958. He received the M.S. and Ph.D. degrees in electrical and computer engineering from the University of Kansas, Lawrence, in 1982 and 1985, respectively.

From November 1985 to December 1987, he was a Post-Doctoral Research Associate at the Center for Research Inc., University of Kansas, where he was involved with microwave remote sensing and computational electromagnetics. In 1988, he joined the Department of Communication Engineering, National Chiao Tung University, Hsinchu, Taiwan, R.O.C., where he is currently a Professor. His current research interests include computational electromagnetics, biological effects and medial applications of electromagnetic energy, and electromagnetic compatibility.

David Wen-Fong Su was born in Kauhsiung, Taiwan, R.O.C., on May 9, 1968. He received the B.S. and M.S. degrees in communications engineering, and the Ph.D. degree from the National Chiao Tung University, Hsinchu, Taiwan, R.O.C., in 1990 and 1992, and 1999, respectively.

From 1992 to 1993, he was a Research and Development Engineer at the Taiwan Microwave Co. Ltd., where he participated in various RF and microwave-circuit-design projects. From 1993 to 1998, he was with the Department of Communication Engineering, National Chiao Tung University, where he was engaged in microwave hyperthermia and radiometry, and traveling-wave tube and insulated antenna design. He is currently with Alpha Telecom Inc., Ksinchu, Taiwan, R.O.C., where he is mainly concerned with the developments of wireless local loop and mobile communication systems.